Order-of-Arrival of Tagged Objects

This is the post peer-review accepted manuscript of:

S. Bartoletti, N. Decarli, D. Dardari, M. Chiani and A. Conti, "Order-of-Arrival of Tagged Objects," in *IEEE Journal of Radio Frequency Identification*, vol. 2, no. 4, pp. 185-196, Dec. 2018.
doi: 10.1109/JRFID.2018.2881708,

The published version is available online at:

URL: http://ieeexplore.ieee.org/stamp/stamp.jsp?tp=&arnumber=8538014&isnumber=8627910

Order-of-Arrival of Tagged Objects

Stefania Bartoletti, *Member, IEEE*, Nicolò Decarli, *Member, IEEE*, Davide Dardari, *Senior Member, IEEE*, Marco Chiani, *Fellow, IEEE*, and Andrea Conti, *Senior Member, IEEE*

***Abstract*—The order-of-arrival (OOA) of a stream of objects moving along a monitored direction is important for many decision operations in logistic and industrial applications. As an example, the dispatch of luggage in airports requires to determine their OOA at checkpoints; as another example, the automatic steering of items in supply chains requires to sort and identify them while moving on a conveyor belt. This paper establishes a general framework for determining the OOA of objects that are moving along a monitored direction via radio-frequency identification (RFID) systems. Three techniques for OOA tracking are proposed and developed for objects equipped with RFID tags possessing ranging capabilities. The benefits of the proposed techniques are experimentally validated based on measurements gathered with a RFID system operating in an indoor environment.**

***Index Terms*—Sorting, tracking, multi-hypothesis testing, RFID, localization.**

I. Introduction

Location awareness plays a key role for various applications in different sectors, including intelligent transportation, and autonomous logistics (the so-called Industry 4.0). As an example, network localization and navigation is employed for handling goods in warehouses, in the automatic steering of items in supply chains, and in the routing of luggage in airports. The sorting and tracking of goods and things moving along a known trajectory, is an essential process for all the aforementioned applications and is referred to as order-of-arrival (OOA) tracking [1]–[3].

To determine the OOA of a stream of objects, each object is detected and identified within the stream and then they are sorted in the direction of movement for successful dispatch or delivery. To this aim, they are equipped with one or more tag devices. The OOA for a stream of objects is a sequential decision problem, where the decision is made with respect to multiple hypotheses representing all the possible ordering, while the sequentiality is given by the update of the decision over time [4]. The filtering of multiple measurements gathered at different time instants enables the refinement of the ordering decision over time. In the following, we will refer to this problem as OOA tracking.

Stefania Bartoletti and Andrea Conti are with the Department of Engineering and CNIT at the University of Ferrara, Ferrara, Italy, E-mail: stefania.bartoletti@unife.it, a.conti@ieee.org

Nicolò Decarli, Davide Dardari, and Marco Chiani are with DEI "Guglielmo Marconi" at the University of Bologna, Cesena, Italy, E-mail: nicolo.decarli@unibo.it, davide.dardari@unibo.it, marco.chiani@unibo.it

This work has received funding from the EU Horizon 2020 research and innovation programme under the Marie Skłodowska-Curie (grant no. 703893) and the project XCycle (grant no. 635975).

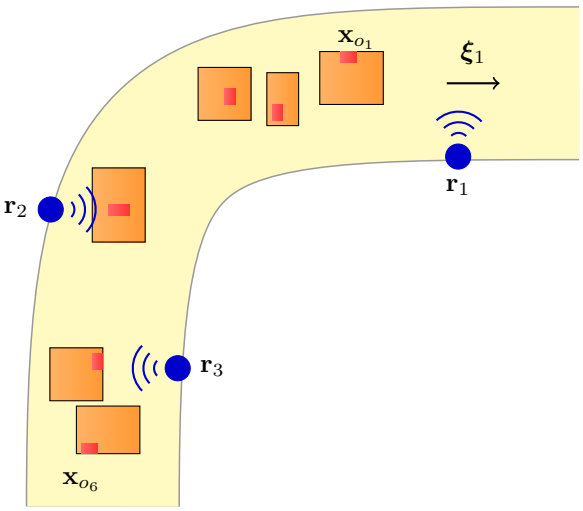

Fig. 1. Top view of a monitored area in a conveyor belt; tags are represented by red rectangles on the objects, the readers are in position $\mathbf{r}_1$, $\mathbf{r}_2$, and $\mathbf{r}_3$. Note that tags can be located on any face of the objects.

Current solutions employ barcode laser scanners, camera barcode readers, vision systems, and RFID readers [5]–[7]. Localization with Gen-2 ultra-high frequency (UHF) RFIDs is based on received signal strength indicator (RSSI), phase (also at different operating frequencies), or angle-of-arrival (AOA) measurements [8]–[14]. The ultra-wideband (UWB) technology [15]–[20] has been recently proposed for new generation RFID systems as it provides high ranging accuracy even in harsh propagation environments [21]–[25]. UWB-based RFID systems rely on the exploitation of the backscatter modulation[1] and the measurement of the time-of-arrival (TOA) of the backscattered signals [26]–[28]. Fig. 1 illustrates an example of ordering system for tagged objects moving on a conveyor belt.

The capability of a system to succeed in determining the OOA in a stream of objects depends on both the *workload conditions* (i.e., number of objects in the monitored area, stream velocity, sorting rate, and minimum distance between consecutive objects) and the *network intrinsic properties* (network topology, wireless medium, and communication and localization signalling). As for the workload conditions, the distance among objects, the speed, and the update rate for identification and sorting are key parameters for the OOA tracking

[1]The tag is powered by the interrogation signal transmitted by the infrastructure composed of interrogation devices (readers).

and its efficiency. As for the network intrinsic properties, the quality of communication between the tag and reader heavily impacts the success probability of determining the OOA of the stream. For example, in range-based OOA tracking, the quality of the range estimates is affected by wireless propagation conditions such as multipath and non-line-of-sight (NLOS) conditions due to other objects obstructing the path between the reader and the tag [29]–[37].

To the authors' knowledge, there are only a few studies related to the OOA via RFID systems, and they focus on specific issues such as workload conditions [5]. However, a mathematical framework to determine the sorting performance accounting for all the aforementioned aspects is not available. Such a framework would serve to design signal processing techniques jointly considering workload conditions and network intrinsic properties as well as to get insights on the main parameters affecting the performance.

In this paper, a framework for design and analysis of systems aiming to track the OOA of a stream of objects is developed. The sorting decision problem is addressed and a tractable model for devising low-complexity solution is derived. The main contributions of the paper can be summarized as follows:

- the introduction of a general framework for OOA tracking via RFID systems;
- the proposal of an energy profile-based Bayesian filtering for OOA tracking;
- the comparison of the proposed energy profile-based method with range-based algorithms;
- the experimental validation of the proposed framework and signal processing is provided for a case study with UWB-UHF RFID.

The remainder of the paper is organized as follows. Sec. II formulates the problem; Sec. III introduces the general framework; Sec. V proposes three location-based algorithms for processing for UWB-UHF RFID; Sec. VI presents the case study; and, finally, Sec. VII gives our conclusion.

Notation: The $\|\mathbf{x}\|$ indicates the norm of the vector $\mathbf{x}$ and $|\cdot|$ denotes the cardinality of a discrete set or the measure of a continuous and measurable set. The $\mathbb{P}\{\mathcal{A}\}$ indicates the probability of the event $\mathcal{A}$. The $\delta(\mathbf{x},\mathbf{q})$ represents the Hamming distance between the vectors $\mathbf{x}$ and $\mathbf{q}$ (i.e., the number of elements for which they differ from each other). The function $f(x|y)$ represents the probability density function (PDF) of the random variable (RV) X conditional on the RV Y calculated at $X=x$ and $Y=y$. Table I defines the main symbols used throughout the paper.

II. Problem Formulation

The problem of tracking the OOA of tagged objects is now formulated: first, the network model is presented, then the performance metrics are defined.

A. Network Model

To easily account for curvilinear streams, consider a conveyor belt carrying N_o objects laying on its surface $\mathcal{A}_\mathrm{c}\subset\mathbb{R}^2$. The objects are indexed by the set $\mathcal{O}=\{1,2,\ldots,N_\mathrm{o}\}$. The ith object is equipped with a tag located at $\mathbf{x}_i^{(k)}=[x_{i,1}^{(k)},x_{i,2}^{(k)},x_{i,3}^{(k)}]\in\mathcal{V}\subset\mathbb{R}^3$ at time t_k, where $\mathcal{V}=\mathcal{A}_\mathrm{c}\times(0,h_\mathrm{max}]$ depends on the conveyor surface and objects' maximum height h_max. The conveyor is monitored by N_r readers indexed by the set $\mathcal{R}$. The rth reader is located at $\mathbf{r}_l\in\mathbb{R}^3$. The readers transmit interrogation signals to detect, identify, and localize the tags in the monitored area.[2] Fig. 1 illustrates an example of conveyor with $\mathcal{R}=\{1,2,3\}$.

The mobility of the conveyor is described by the trajectory

$$\mathbf{x}_i^{(2)}=\mathbf{c}(\mathbf{x}_i^{(1)},t_2-t_1) \tag{1}$$

which represents the position at time $t_2\geq t_1$ of the ith tag moving from $\mathbf{x}_i^{(1)}\in\mathcal{V}$ at time t_1. As an exemplifying case, consider the case of constant velocity vector $\dot{\mathbf{x}}_i^{(k)}(t)=[v,0,0]\ \forall k$, and a rectilinear stream for which $\mathbf{x}_i^{(2)}=\mathbf{c}(\mathbf{x}_i^{(1)},t_2-t_1)=\mathbf{x}_i^{(1)}+[v(t_2-t_1),0,0]$.

Consider a coordinate chart that maps the Cartesian coordinate $\mathbf{x}_i^{(k)}\in\mathbb{R}^3$ into the curvilinear coordinate $\boldsymbol{\xi}_i^{(k)}=\xi_{i,1}^{(k)}\boldsymbol{\xi}_1+\xi_{i,2}^{(k)}\boldsymbol{\xi}_2+\xi_{i,3}^{(k)}\boldsymbol{\xi}_3$, where $\boldsymbol{\xi}_1,\boldsymbol{\xi}_2$ and $\boldsymbol{\xi}_3$ are the local basis vectors for the curvilinear coordinate system.[3] The curvilinear system is defined such that the first vector $\boldsymbol{\xi}_1$ changes direction point to point according to the conveyor direction. Based on this definition, the first coordinate of the curvilinear system determines the OOA of the N_o tagged objects. In particular, the mapping between the Cartesian coordinate $\mathbf{x}_i^{(k)}$ and the first curvilinear coordinate $\xi_{i,1}^{(k)}$ is defined through the map function $m:\mathbb{R}^3\to\mathbb{R}$ as

$$\xi_{i,1}^{(k)}=m\big(\mathbf{x}_i^{(k)}\big)\,. \tag{2}$$

In the exemplifying case with $\dot{\mathbf{x}}(t)=[v,0,0]$, the local basis vectors are $\boldsymbol{\xi}_1=\mathbf{b}_1$, $\boldsymbol{\xi}_2=\mathbf{b}_2$, and $\boldsymbol{\xi}_3=\mathbf{b}_3$, where $\mathbf{b}_1$, $\mathbf{b}_2$, and $\mathbf{b}_3$ are the basis vector for the Cartesian coordinate system. The mapping is $\xi_{i,1}^{(k)}=m\big(\mathbf{x}_i^{(k)}\big)=x_{i,1}^{(k)}$ and we are interested in ordering the vector $[x_{1,1}^{(k)},x_{2,1}^{(k)},\ldots,x_{N_\mathrm{o},1}^{(k)}]$ at time t_k. By means of (2) one can model any stream shape as a 1-D rectilinear case and then remap the results into the initial geometry.

In the general case, the OOA of the objects is represented by the vector $\mathbf{o}=[o_1,o_2,\ldots,o_{|\mathcal{O}|!}]$, whose hth element $o_h=l$ indicates that the lth object is the hth along the conveyor direction, i.e.,

$$o_h=\underset{i\notin\{o_1,\ldots,o_{h-1}\}}{\operatorname{argmax}}\left\{\xi_{i,1}^{(k)}\,:\,i\in\mathcal{O}\right\}\,. \tag{3}$$

Note that if the conveyor mobility described in (1) is deterministic and known exactly, the tag position can be determined at any time based on its initial position and the elapsed time. Therefore, the vector $\mathbf{o}$ does not depend on the time index k.

The OOA tracking consists of (i) detecting the interrogated tags and (ii) estimating their OOA. In general, a subset $\mathcal{D}\subset\mathcal{O}$ is detected among those interrogated, therefore we define

[2] In case of multiple tags per object, the extended model is straightforward, by defining the object position as a function of the corresponding tags' positions (e.g., spatial averaging).

[3] A basis whose vectors change their direction from point to point is called a local basis. Basis vectors that are the same at all points are global bases, and can be associated only with linear or affine coordinate systems. Lee:B13

TABLE I
MAIN SYMBOLS USED THROUGHOUT THE PAPER

Symbol	Description	Symbol	Description
N_o	number of objects	$\mathbf{z}$	vector of measurements from the network of readers
$\mathcal{A}_\mathrm{c}$	surface area of the conveyor	Ω_j	set of possible ordering for $\lvert\mathcal{D}\rvert = j$
$\mathcal{O}$	index set of the object	$f(\mathbf{z}\lvert\mathbf{o})$	PDF of the measurements given $\mathbf{o}$
$\mathbf{x}_i^{(k)}$	position of the tag for the ith object at time k in the Cartesian coordinate system	$\Lambda(\mathbf{o}\lvert\mathbf{z})$	likelihood function for $\mathbf{o}$ given the measurement vector
$\boldsymbol{\xi}_i^{(k)}$	position of the tag of the tag for the ith object at time k in the curvilinear coordinate system	$\mathbf{H}_\mathbf{x}(g(\mathbf{x}))$	Hessian matrix of $g(\mathbf{x})$ with respect to $\mathbf{x}$
$m(\cdot)$	map function from the Cartesian to the curvilinear coordinate system	$\delta(\mathbf{p},\mathbf{q})$	Hamming distance between $\mathbf{p}$ and $\mathbf{q}$
$\mathbf{o}$	vector representing the OOA of the objects	$\boldsymbol{\tau}^{(k)}$	vector of estimated TOAs at time index k
$\mathcal{D}$	index set of detected objects	$\mathbf{b}^{(k)}$	vector of energy samples at time index k

$\mathbf{o}_\mathrm{d}$ as the OOA vector related only to the detected objects. For example if $\mathbf{o} = [5,2,1,3,4]$ and $\mathcal{D} = \{1,3,5\}$ then $\mathbf{o}_\mathrm{d} = [5,1,3]$. Therefore, the estimated OOA vector $\widehat{\mathbf{o}}_\mathrm{d}$ is an estimate of $\mathbf{o}_\mathrm{d}$. The detection and estimation phases rely on a set $\mathbf{z} = \left\{\mathbf{z}_r^{(k)}\right\}$ of measurements taken by the network of readers, where $\mathbf{z}_r^{(k)}$ is the set of measurements taken by the rth reader at time index $k = 1,2,\ldots,N_\mathrm{m}$ within an observation interval $T_\mathrm{obs} = N_\mathrm{m}T$; N_m is the number of measurements; and T is the time interval between two subsequent measurements from the same reader. For example, the measurements can be the samples of the signal communicated between the reader and the interrogated tags in a RFID system. The number of measurements N_m and therefore the observation time impact the sorting time of the system (together with the number of interrogated tags and the number of readers, especially if the signal processing is centralized).

B. Detection and Ordering

If the detection and ordering problems are considered jointly, the OOA can take value within a set $\breve{\Omega} = \bigcup_{j=1}^{N_\mathrm{o}} \Omega_j \cup \emptyset$ where Ω_j is the set of possible ordering for $\lvert\mathcal{D}\rvert = j$. In particular, there are $\binom{N_\mathrm{o}}{j}$ possible grouping of elements in $\mathcal{D}$ and $j!$ possible permutations of the elements in $\mathbf{o}$ given $\mathcal{D}$ when $\lvert\mathcal{D}\rvert = j$. In total, the number of possible results of the OOA tracking is

$$\left|\breve{\Omega}\right| = \sum_{j=0}^{N_\mathrm{o}} \frac{N_\mathrm{o}!}{(N_\mathrm{o}-j)!} \tag{4}$$

which grows exponentially with N_o. For example, if $N_\mathrm{o} = 3$ then $i \in \mathcal{O} = \{1,2,3\}$; $\breve{\Omega} = \emptyset \cup \{[1],[2],[3],[1,2],[2,1],[1,3],[3,1],[3,2],[2,3],[1,2,3],[1,3,2],[2,1,3],[2,3,1],[3,1,2],[3,2,1]\}$, which corresponds to $\left|\breve{\Omega}\right| = 16$ as given by (4). Then, the detection and estimation problem corresponds to an M-ary hypothesis test with $M = \left|\breve{\Omega}\right|$, where

$$\begin{aligned} &\mathcal{H}_0 : \mathbf{o} = \emptyset \\ &\mathcal{H}_i : \mathbf{o} = \boldsymbol{\omega}_i \quad \forall\, \boldsymbol{\omega}_i \in \breve{\Omega}\backslash\emptyset\,. \end{aligned} \tag{5}$$

In case of ordering after detection (i.e., the detection and ordering problem are treated sequentially), the hypothesis test can be substantially simplified given the set $\mathcal{D}$ of detected objects and the number of hypotheses decreases significantly with respect to the case where the detection and ordering are treated jointly. Therefore, in the following the detection and sorting problems are considered sequentially for computational complexity reasons.

Given $\mathcal{D}$, the estimated order vector $\mathbf{o}_\mathrm{d}$ can take $\lvert\mathcal{D}\rvert!$ possible values $\mathbf{o}_\mathrm{d} \in \Omega_\mathrm{d} = \left\{\boldsymbol{\omega}_1, \boldsymbol{\omega}_2, \ldots, \boldsymbol{\omega}_{\lvert\mathcal{D}\rvert!}\right\}$, with $\boldsymbol{\omega}_i = [\omega_{i1}, \omega_{i2}, \ldots, \omega_{i\lvert\mathcal{D}\rvert}]$.[4] Therefore, the estimated OOA $\widehat{\mathbf{o}}_\mathrm{d}$ can take $\lvert\mathcal{D}\rvert!$ possible outcomes $\widehat{\mathbf{o}}_\mathrm{d} \in \Omega_\mathrm{d} = \left\{\boldsymbol{\omega}_1, \boldsymbol{\omega}_2, \ldots, \boldsymbol{\omega}_{\lvert\mathcal{D}\rvert!}\right\}$. For example, if $\mathbf{o} = [5,2,1,3,4]$ and $\mathcal{D} = \{1,3,5\}$ then $\Omega_\mathrm{d} = \{[1,3,5],[1,5,3],[3,1,5],[3,5,1],[5,1,3],[5,3,1]\}$.

This corresponds to an M-ary hypothesis test with $M = \lvert\mathcal{D}\rvert!$ where the jth hypothesis is

$$\mathcal{H}_j : \mathbf{o}_\mathrm{d} = \boldsymbol{\omega}_i \quad \forall i \in \Omega_\mathrm{d}\,. \tag{6}$$

C. Performance Metrics

The system succeeds in ordering a stream of objects, when the detected elements of the vector $\mathbf{o}$ are successfully ordered in the vector $\widehat{\mathbf{o}}_\mathrm{d}$. The success probability is

$$P_\mathrm{s}(\mathbf{o}_\mathrm{d}) = 1 - \sum_{i=1}^{\lvert\mathcal{D}\rvert!} \frac{\delta(\mathbf{o}_\mathrm{d}, \boldsymbol{\omega}_i)}{\lvert\mathcal{D}\rvert} \mathbb{P}\left\{\widehat{\mathbf{o}}_\mathrm{d} = \boldsymbol{\omega}_i \lvert \mathbf{o}_\mathrm{d}\right\} \tag{7}$$

where $\delta(\mathbf{p},\mathbf{q})$ denotes the Hamming distance (i.e., the number of elements in which two vectors differs from each other) between $\mathbf{p}$ and $\mathbf{q}$.

To provide a performance benchmark for the success probability in (7), we approximate $\mathbb{P}\{\widehat{\mathbf{o}} = \boldsymbol{\omega}_i\}$ for large sample size $\lvert\mathbf{z}\rvert$. In particular, given $\mathbf{o} = \boldsymbol{\omega}_i$

$$\mathbb{P}\left\{\widehat{\mathbf{o}} = \boldsymbol{\omega}_j\right\} = \mathbb{P}\left\{\text{decide } \mathcal{H}_j \lvert \mathcal{H}_i\right\} \simeq \mathbb{P}\left\{\hat{\mathbf{x}}_{0,i} \in \mathcal{P}_j \lvert \mathcal{H}_i\right\}\,. \tag{8}$$

It is known that, given the true value $\mathbf{x}$, the maximum likelihood estimator converges in distribution as

$$\sqrt{\lvert\mathbf{z}\rvert}(\hat{\mathbf{x}}_{0,i} - \mathbf{x}) \sim \mathcal{N}(0, \mathbf{I}^{-1}) \tag{9}$$

where $\mathbf{I}$ is the Fisher information matrix [4], [17]. Therefore

$$P_\mathrm{s}(\mathbf{o}) \simeq 1 - \sum_{i=1}^{\lvert\mathcal{D}\rvert!} \frac{\delta(\mathbf{o}_\mathrm{d}, \boldsymbol{\omega}_i)}{\lvert\mathcal{D}\rvert} \frac{1}{\lvert\mathcal{P}_i\rvert} \int_{\mathcal{P}_i} \int_{\mathcal{P}_j} \phi\left(\tilde{\mathbf{x}} \middle| \mathbf{x}, \frac{\mathbf{I}^{-1}}{N}\right) d\tilde{\mathbf{x}} d\mathbf{x} \tag{10}$$

where $\phi(x|\mu,\sigma^2)$ is the probability density function of a Gaussian RV with mean μ and variance σ^2.

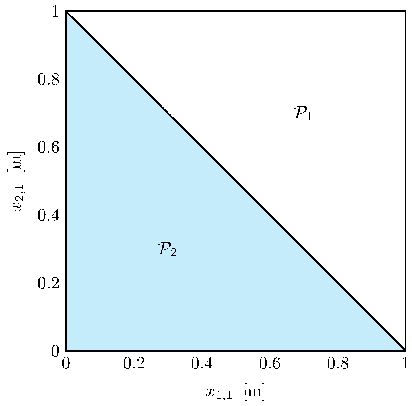

Fig. 2. Example illustration for $\mathcal{P}_1$ and $\mathcal{P}_2$ defined by $x_{1,1}$ and $x_{2,1}$ when $N_\mathrm{o}=2$ and $\mathbf{x}_i = x_{i,1} \in \mathbb{R}$. If $\mathbf{x} = [\xi_1, \xi_2] \in \mathcal{P}_1$, then $\mathbf{o} = \boldsymbol{\omega}_1 = [1,2]$, whereas if $\mathbf{x} \in \mathcal{P}_2$ then $\mathbf{o} = \boldsymbol{\omega}_2 = [2,1]$.

III. OOA Tracking

The decision process for the OOA tracking is now described.

Define $\mathbf{x}^{(k)} = [\mathbf{x}_1^{(k)}, \mathbf{x}_2^{(k)}, \ldots, \mathbf{x}_{|\mathcal{D}|}^{(k)}]$ as the vector of the detected but unknown tags' positions at time k. All the possible values of $\mathbf{x}^{(k)}$ are contained in a subspace $\mathcal{P} \subset \mathbb{R}^{3|\mathcal{D}|!}$.[5] Specifically, the values of $\mathbf{x}^{(k)}$ for which $\mathbf{o}_i = \boldsymbol{\omega}_i$ belong to a subspace

$$\mathcal{P}_i = \Big\{ \mathbf{x}^{(k)} \text{ s.t. } m(\mathbf{x}^{(k)}_{\omega_{i,1}}) \le m(\mathbf{x}^{(k)}_{\omega_{i,2}}) \le \ldots \\ m(\mathbf{x}^{(k)}_{\omega_{i,(N_\mathrm{o}-1)}}) \le m(\mathbf{x}^{(k)}_{\omega_{i,N_\mathrm{o}}}) \Big\} . \tag{11}$$

with $\mathcal{P}_i \subset \mathcal{P}$ and $\mathcal{P}_i \cap \mathcal{P}_j = \emptyset$. Then, the hypothesis test is

$$\mathcal{H}_i : \mathbf{x}^{(k)} \in \mathcal{P}_i \tag{12}$$

where the hypotheses are composite and non-nested with respect to the parameter $\mathbf{x}^{(k)}$. For example, when $N_\mathrm{o} = 2$ and $m(\mathbf{x}_i^{(k)}) = x_{i,1}^{(k)}$ the binary hypothesis testing is

$$\begin{aligned} \mathcal{H}_1 &: \mathbf{x}^{(k)} \in \mathcal{P}_1 \\ \mathcal{H}_2 &: \mathbf{x}^{(k)} \in \mathcal{P}_2 \end{aligned} \tag{13}$$

with $\mathcal{P}_1 = \left\{ [\mathbf{x}_1^{(k)}, \mathbf{x}_2^{(k)}] : x_{i,1}^{(k)} \le x_{i,2}^{(k)} \right\}$ and $\mathcal{P}_2 = \left\{ [\mathbf{x}_1^{(k)}, \mathbf{x}_2^{(k)}] : x_{i,2}^{(k)} < x_{i,1}^{(k)} \right\}$. Fig. 2 illustrates the case with $\mathbf{x}_i^{(k)} = x_{i,1}^{(k)} \in \mathbb{R}$.

Following a likelihood-based approach, given a dataset $\mathbf{z}$ of observations the estimation of the order vector is $\widehat{\mathbf{o}} = \boldsymbol{\omega}_i$

$$\hat{\imath} = \underset{i}{\operatorname{argmax}}\, \mathbb{P}\{\mathbf{z}|\mathcal{H}_i\} = \underset{i}{\operatorname{argmax}}\, \Lambda(\boldsymbol{\omega}_i|\mathbf{z}) \tag{14}$$

where $\Lambda(\boldsymbol{\omega}_i|\mathbf{z})$ is the likelihood function of the vector $\mathbf{z}$ for the ith hypothesis.

Consider $\mathbf{z} = \left[\mathbf{z}^{(1)}, \mathbf{z}^{(2)}, \ldots, \mathbf{z}^{(N_\mathrm{m})}\right]$, where $\mathbf{z}^{(k)}$ contains the measurements $\mathbf{z}_{l,j}^{(k)}$ with $l \in \mathcal{R}$ and $j \in \mathcal{D}$ taken by the lth receiver for the jth tag at time k. In particular, we consider the measurements taken for each reader-tag link as independent.[6] Based on the relation between $\mathbf{o}$ and $\mathbf{x}^{(k)}$, the likelihood function becomes

$$\begin{aligned} \Lambda(\boldsymbol{\omega}_i|\mathbf{z}) &= f(\mathbf{z}|\boldsymbol{\omega}_i) = \int_{\mathcal{P}} f(\mathbf{z}|\mathbf{x}) f(\mathbf{x}|\boldsymbol{\omega}_i) d\mathbf{x} \\ &= \frac{1}{|\mathcal{P}_i|} \int_{\mathcal{P}_i} f(\mathbf{z}|\mathbf{x}) d\mathbf{x} \end{aligned} \tag{15}$$

with equal probability for each $\boldsymbol{\omega}_i$ and for each $\mathbf{x} \in \mathcal{P}_i$ given $\mathbf{o} = \boldsymbol{\omega}_i$. The likelihood function can be rewritten as an explicit function of $\mathbf{x}_i$ as

$$\begin{aligned} \Lambda(\boldsymbol{\omega}_i|\mathbf{z}) = \prod_{k=1}^{N_\mathrm{m}} \int_{\mathcal{V}} \ldots \int_{\mathcal{V}} \prod_{l\in\mathcal{R}} \prod_{j\in\mathcal{D}} f(\mathbf{z}_{l,\omega_{i,j}}^{(k)} | \mathbf{x}_{\omega_{i,j}}) \\ \times f(\mathbf{x}_{\omega_{i,1}}, \ldots, \mathbf{x}_{\omega_{i,|\mathcal{D}|}} | \boldsymbol{\omega}_i) d\mathbf{x}_{\omega_{i,1}}, \ldots, d\mathbf{x}_{\omega_{i,|\mathcal{D}|}} . \end{aligned} \tag{16}$$

For example, in the binary case described in (13) the likelihood function becomes

$$\begin{aligned} \Lambda(\boldsymbol{\omega}_1|\mathbf{z}) &= \prod_{k=1}^{N_\mathrm{m}} \int_{\mathcal{V}} \int_{\mathcal{V}} \prod_{l\in\mathcal{R}} f(\mathbf{z}_{j,1}^{(k)}|\mathbf{x}_1) f(\mathbf{z}_{j,2}^{(k)}|\mathbf{x}_2) \\ &\quad \times f(\mathbf{x}_1, \mathbf{x}_2|\boldsymbol{\omega}_1) d\mathbf{x}_1 d\mathbf{x}_2 \\ &= \int_{\mathcal{V}} \int_{\mathcal{V}^+(\mathbf{x}_1)} \prod_{l\in\mathcal{R}} \frac{f(\mathbf{z}_{j,1}^{(k)}|\mathbf{x}_1)}{|\mathcal{V}||\mathcal{V}^+(\mathbf{x}_1)|} f(\mathbf{z}_{j,2}^{(k)}|\mathbf{x}_2) d\mathbf{x}_2 d\mathbf{x}_1 \end{aligned} \tag{17}$$

where $\mathcal{V}^+(\mathbf{x}_1) = \{\mathbf{x}_2 \text{ s.t. } x_{21} \ge x_{11}\}$ and we considered uniform distribution over $\mathcal{V}$.

Following a Bayesian approach, the OOA can be estimated through (15) as

$$\widehat{\mathbf{o}} = \underset{\omega_i \in \bar{\Omega}_\mathrm{d}}{\operatorname{argmax}} \int_{\mathcal{P}} f(\mathbf{z}|\mathbf{x}) f(\mathbf{x}|\boldsymbol{\omega}_i) d\mathbf{x} . \tag{18}$$

However, the integrand function is not in closed form as can be seen in (17) for the simple case with $N_\mathrm{o} = 2$. Furthermore, the complexity of the integral computation grows with N_o and limits the update rate of the OOA tracking. Therefore, this solution is of little practical application, and thus a tractable model is required for the system implementation.

IV. Tractable Model for OOA tracking

We now present a Laplace's approximation to derive a tractable expression for (18). Consider the Taylor series expansion for the natural logarithm of the integrand function in (15) around its maximum value $\hat{\mathbf{x}}_{0,i}$ for $\mathbf{x}$

$$\begin{aligned} \log(f(\mathbf{z}|\mathbf{x}) f(\mathbf{x}|\boldsymbol{\omega}_i)) &= \log(f(\mathbf{z}|\hat{\mathbf{x}}_{0,i}) f(\hat{\mathbf{x}}_{0,i}|\boldsymbol{\omega}_i)) \\ &\quad - \frac{1}{2}(\mathbf{x} - \hat{\mathbf{x}}_{0,i})^T \mathbf{Q}_i (\mathbf{x} - \hat{\mathbf{x}}_{0,i}) + O(\mathbf{x}^3) \end{aligned} \tag{19}$$

where

$$\mathbf{Q}_i = -\mathbf{H}_\mathbf{x} \log(f(\mathbf{z}|\hat{\mathbf{x}}_{0,i}) f(\hat{\mathbf{x}}_{0,i}|\boldsymbol{\omega}_i)) \tag{20}$$

and $\mathbf{H}_\mathbf{x} g(\mathbf{x})$ denotes the Hessian matrix of $g(\mathbf{x})$ with respect to $\mathbf{x}$, and the first order term is equal to zero since $\hat{\mathbf{x}}_{0,i}$ is the maximum value for $f(\mathbf{z}|\mathbf{x})$.

[4] For a description of the detection phase related to the case study the reader can refer to [38].

[5] Note that the general definition is $\mathbf{x} \in \mathcal{P} \subset \mathbb{R}^{K\cdot|\mathcal{D}|!}$ if $\mathbf{x}_i \in \mathbb{R}^K$.

[6] This requires perfect suppression of inter-tag interference; the effects of interference among tags are investigated in [38], [39] for the UWB-UHF RFID case.

Note that the point of maximum is $\hat{\mathbf{x}}_{0,i}$, which represents the maximum likelihood estimation for a given hypothesis $\mathcal{H}_i$. In particular,

$$\begin{aligned}\hat{\mathbf{x}}_{0,i} &= \underset{\mathbf{x}}{\operatorname{argmax}}\, f(\mathbf{z}|\mathbf{x}) f(\mathbf{x}|\boldsymbol{\omega}_i) \\ &= \underset{\mathbf{x}\in\mathcal{P}_i}{\operatorname{argmax}}\, f(\mathbf{z}|\mathbf{x}) \end{aligned} \tag{21}$$

where the second equality holds because $f(\mathbf{x}|\boldsymbol{\omega}_i) = 0$ for $\mathbf{x} \notin \mathcal{P}_i$ and assuming uniform distribution $f(\mathbf{x}|\boldsymbol{\omega}_i) = \frac{1}{|\mathcal{P}_i|}$ for $\mathbf{x} \in \mathcal{P}_i$. Since $f(\mathbf{x}|\boldsymbol{\omega}_i)$ does not depend on the sample size $|\mathbf{z}|$, for large $|\mathbf{z}|$ we have $\frac{1}{|\mathbf{z}|}\mathbf{Q}_i \approx O(1)$ and

$$\mathbf{Q}_i \simeq -\mathbf{H}_{\mathbf{x}} \log(f(\mathbf{z}|\hat{\mathbf{x}}_{0,i}))\,. \tag{22}$$

where $\mathbf{H}_{\mathbf{x}}$ is the Hessian operator with respect to $\mathbf{x}$. In addition, $\hat{\mathbf{x}}_{0,i}$ tends to the true value of $\mathbf{x}$ if $\boldsymbol{\omega}_i$ is the true OOA vector $\mathbf{o} = \boldsymbol{\omega}_i$. In these conditions, by using the Laplace's approximation

$$\mathbb{P}\{\mathbf{z}|\mathcal{H}_i\} \simeq \frac{f(\mathbf{z}|\hat{\mathbf{x}}_i)}{|\mathcal{P}_i|}\sqrt{|2\pi\mathbf{Q}_i^{-1}|}\,. \tag{23}$$

From (19) we have

$$\begin{aligned}\log \mathbb{P}\{\mathbf{z}|\mathcal{H}_i\} &\approx \log f(\mathbf{z}|\hat{\mathbf{x}}_{0,i}) - \frac{\log|\mathbf{Q}_i|}{2} + O(1) \\ &= \log f(\mathbf{z}|\hat{\mathbf{x}}_i) - \frac{\log\left(\frac{|\mathbf{z}\mathbf{Q}_i|}{|\mathbf{z}|}\right)}{2} + O(1) \\ &= \log f(\mathbf{z}|\hat{\mathbf{x}}_i) - \frac{|\mathbf{z}|}{2} + O(1) \end{aligned} \tag{24}$$

where the last equation holds since $\frac{\mathbf{Q}_i}{|\mathbf{z}|} \simeq O(1)$ and $O(1)$ includes all the constant terms, which are independent of $|\mathbf{z}|$.

From (19) and (24) it follows that the application of the hypothesis test for the OOA tracking is equivalent to first calculating the maximum likelihood estimation of the position vector $\mathbf{x}$ and then sorting the position estimates along the conveyor direction as

$$\hat{\imath} = \underset{i}{\operatorname{argmax}}\, \mathbb{P}\{\mathbf{z}|\mathcal{H}_i\} \simeq \underset{i}{\operatorname{argmax}} \max_{\mathbf{x}\in\mathcal{P}_i} f(\mathbf{z};\mathbf{x})\,. \tag{25}$$

Remark 1. *The OOA estimation problem is formally reconducted to a localization problem, where the relative position of the objects with respect to the direction of the conveyor is considered. In the general case, the conveyor direction changes over time.*

A. Location-based OOA Tracking

We now consider two approaches for the estimation of $\hat{\mathbf{x}}$ and therefore of $\hat{\mathbf{o}}$. As first approach, we consider the OOA decision as a static process where the estimation is performed without exploiting any prior information on the measurement $\mathbf{z}$. In this case, a range-based least squares (LS) algorithm is considered where $\mathbf{z}_{l,i}^{(k)} = \hat{\tau}_{l,i}^{(k)}$ is the estimated time-of-arrival (TOA) between the rth reader and the jth object at time k, and the estimated position vector is

$$\hat{\mathbf{x}}_{\mathrm{LS}} = \underset{i}{\operatorname{argmin}} \min_{\mathbf{x}\in\mathcal{P}_i} \sum_{l\in\mathcal{R}}\sum_{i\in\mathcal{O}} (\hat{\tau}_{l,i}^{(k)} - \|\mathbf{x}_i - \mathbf{r}_l\|/c)^2\,. \tag{26}$$

As second approach, we consider the OOA tracking as a dynamic process and the stochastic filtering problem. In fact, the processing of multiple measurements gathered at different time instants enables the refinement of the decision over time. The filtering problem is given by [40]

$$\begin{aligned}\mathbf{x}^{(k+1)} &= \mathbf{f}(\mathbf{x}^{(k)}, \mathbf{q}^{(k)}) \\ \mathbf{z}^{(k)} &= \mathbf{g}(\mathbf{x}^{(k)}, \mathbf{c}^{(k)}) \end{aligned} \tag{27}$$

that are the state equation and measurement equation, respectively. Note that $\mathbf{q}^{(k)}$ and $\mathbf{c}^{(k)}$ are noise random sequences (dynamical noise and measurement noise, respectively) with unknown statistics in a general case.

For example, in the example of constant velocity vector $\dot{\mathbf{x}}(t) = [v, 0, 0]$, and rectilinear stream for which $\mathbf{x}(t_2) = \mathbf{c}(\mathbf{x}(t_1), t_2 - t_1) = \mathbf{x}(t_1) + [v(t_2 - t_1), 0, 0]$. we have the state equation

$$\mathbf{x}^{(k+1)} = \mathbf{x}^{(k)} + vT + \mathbf{q}^{(k)} \tag{28}$$

where $\mathbf{q}^{(k)}$ is the noise related to the dynamics of the conveyor.

Following a Bayesian approach, the state and measurement equations are used to calculate the density function $f(\mathbf{z}^{(1:k)}|\mathbf{x}^{(k)})$ through two phases (i.e., prediction and update) at each time index k (e.g., via particle filtering or Kalman filtering). In particular, the vector estimate $\widehat{\mathbf{x}}^{(k)}$ is determined as the value that maximizes the position belief $b(\mathbf{x}^{(1:k)}) = f(\mathbf{x}^{(1:k)}|\mathbf{z}^{(1:k)}) \propto f(\mathbf{z}^{(k)}|\mathbf{x}^{(k)}) f(\mathbf{x}^{(k)}|\mathbf{x}^{(k-1)})$, which is the posterior distribution of the state vector given the observation vector. Note that such distributions are derived by relying on the (27) and (28). Mobility and measurement models are used to predict, update, and resample the position belief at each k. In particular, a Gaussian mobility model is given by

$$f(\mathbf{x}^{(k)}|\mathbf{x}^{(k-1)}) = \frac{1}{\sqrt{2\pi}\sigma_{\mathrm{m},k}} \prod_{i\in\mathcal{D}} e^{-\frac{\left\|\mathbf{x}_i^{(k)} - \widehat{\boldsymbol{\mu}}_i^{(k)}\right\|^2}{2\sigma_{\mathrm{m},k}^2}} \tag{29}$$

where $\sigma_{\mathrm{m},k}^2$ depends on the conveyor noise $\mathbf{q}^{(k)}$ in (28) and $\widehat{\boldsymbol{\mu}}_i^{(k)} = \mathbf{c}(\mathbf{x}^{(k-1)}, T)$. The measurement model is $f(\mathbf{z}^{(k)}|\mathbf{x}^{(k)})$ and depends on the type of measurement $\mathbf{z}^{(k)}$. We will consider two cases with different $\mathbf{z}^{(k)}$ for the UWB-UHF RFID in Sec. V.

V. OOA Tracking for UWB-UHF RFID

The type of measurement $\mathbf{z}$ that is used for OOA tracking depends on the system employed, e.g. range-based estimation, optical reading. In this paper, we focus on a UHF-UWB RFID system, where $\mathbf{z}$ is collected via energy detection. The system architecture and an energy profile-based Bayesian filter (BF) are now presented.

A. System Architecture

The considered UHF-UWB RFID system is depicted in Fig. 3 and was proposed in [38]. In this system, the reader is the only device with capability of transmitting, receiving, and processing signals, whereas tags are passive reflectors. Each reader consists of a joint UHF-UWB transmitting/receiving unit designed to enable network synchronization, tag detection

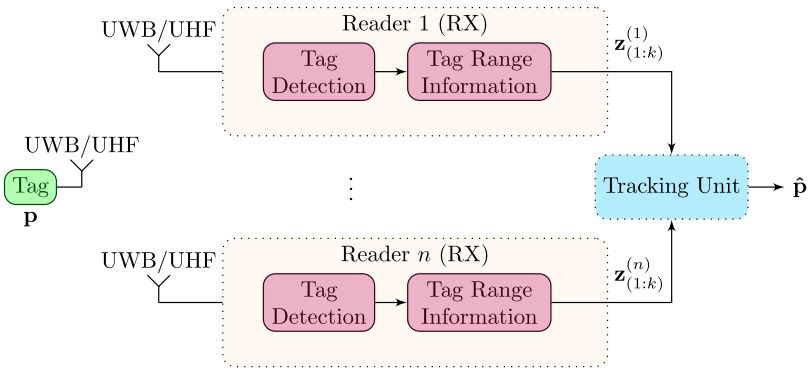

Fig. 3. Example of UHF-UWB reader-tag communications.

Algorithm 1 Range-based Least Square

for $k = 1, 2, \ldots$ **do**
  for $l \in \mathcal{R}$ **do**
    Energy Detection: $\mathbf{b}_l^{(k)} \leftarrow r_l^{(k)}(t)$
    Decision Algorithm: $\hat{\boldsymbol{\tau}}_{l,i}^{(k)} \leftarrow \mathbf{b}_{l,i}^{(k)}$
  LS: $\mathbf{x}_{\text{LS}}^{(k)} \leftarrow \hat{\boldsymbol{\tau}}^{(k)}$ from (26)
  Sorting: $\hat{\mathbf{o}} \leftarrow \mathbf{x}_{\text{LS}}^{(k)}$

Algorithm 2 Range-based Particle Filter

for $k = 1, 2, \ldots$ **do**
  for $l \in \mathcal{R}$ **do**
    Energy Detection: $\mathbf{b}_i^{(k)} \leftarrow r_l^{(k)}(t)$
    Decision Algorithm: $\hat{\boldsymbol{\tau}}_{l,i}^{(k)} \leftarrow \mathbf{b}_{l,i}^{(k)}$
  procedure BAYESIAN FILTER
    Update: $f(\mathbf{x}^{(k)}|\boldsymbol{\tau}^{(1:k)}) \leftarrow \hat{\boldsymbol{\tau}}^{(k)}$
    $\hat{\mathbf{x}}^{(k)} \leftarrow \text{argmax}_{\mathbf{x}^{(k)}} f(\mathbf{x}^{(k)}|\boldsymbol{\tau}^{(1:k)})$
    Prediction: $f(\mathbf{x}^{(k+1)}|\boldsymbol{\tau}^{(1:k)}) \leftarrow \boldsymbol{\tau}^{(1:k-1)}$
  Sorting: $\hat{\mathbf{o}} \leftarrow \hat{\mathbf{x}}^{(k)}$

Algorithm 3 Energy profile-based Bayesian Filter

for $k = 1, 2, \ldots$ **do**
  for $r \in \mathcal{R}$ **do**
    Energy Detection: $\mathbf{b}_i^{(k)} \leftarrow \mathbf{r}_i^{(k)}$
  procedure BAYESIAN FILTER
    Update: $f(\mathbf{x}^{(k)}|\mathbf{b}^{(1:k)}) \leftarrow \mathbf{b}^{(1:k)}$
    $\hat{\mathbf{x}}^{(k)} \leftarrow \text{argmax}_{\mathbf{x}^{(k)}} f(\mathbf{x}^{(k)}|\mathbf{b}^{(1:k)})$
    Prediction: $f(\mathbf{x}^{(k)}|\mathbf{b}^{(1:k)}) \leftarrow \boldsymbol{\tau}^{(1:k-1)}$
  Sorting: $\hat{\mathbf{o}} \leftarrow \hat{\mathbf{x}}^{(k)}$

and identification, and range-information extraction for OOA tracking. The UHF link serves for both network synchronization and reader-tag data communication (e.g., using a standard Gen-2 protocol), while the UWB link serves for reader-tag ranging and tag-to-reader data transmission [24]. The reader is composed of the transmitter section, which emits periodic interrogation signals, and the receiver section, which analyzes the received UWB backscattered signals to detect tags located in the monitored area.

Tags are equipped with a UHF and a UWB section. The former allows the reader-tag communication through UHF backscatter modulation as in standard Gen-2 tags, the powering up, and the synchronization of the UWB backscatter modulator [21]. The latter is a backscatter modulator that switches the UWB antenna between two load conditions for creating a unique tag to reader channel for communication and ranging [24]. Each receiver can accumulate several UWB pulses N_{pulse} to reach the SNR required for obtaining a reliable reader-tag communication. The minimum value of N_{pulse} depends on the desired operating range, and the amount of time for detection and demodulation of signals backscattered by tags increases with N_{pulse} (i.e., lower refresh rate) [24]. For example, the accumulation of $N_{\text{pulse}} = 8192$ pulses increases the SNR of 39 dB with respect to $N_{\text{pulse}} = 1$, but it also increases the amount of time for detection of 1 ms.

The OOA tracking relies on the processing of the signals received back at each reader. In particular, from the signal received at the lth reader, a vector of observations $\mathbf{z}_{l,i}^{(k)}$ is obtained by extracting the range information related to the ith tag at time index k. The OOA is estimated by jointly processing the observation vectors related to all the N_{o} objects.

B. Energy profile-based Bayesian filtering

The UWB signal $r_l^{(k)}(t)$ is received by the lth reader at time index k and processed as shown in Fig. 4. After band-pass filtering and despreading for extracting the signal component backscattered by the ith tag, the received signal is processed by an energy detector, which squares and integrates the received waveform over subsequent dwell time intervals of duration T_{dwell} to obtain a vector of energy bins $\mathbf{b}^{(k)}$ [29]. The elements of the energy vector $\mathbf{b}^{(k)}$ at the output of the energy detector $e_{i,j,m}^{(k)}$ are instantiation of RVs $\mathbf{b}_{i,j,m}^{(k)}$, which are distributed as non-central chi-squared random variables $\mathbf{b}_{i,j,m}^{(k)} \sim \chi_K^2(\lambda_{i,j,m}^{(k)})$ when conditional on the channel impulse response. K is the number of degrees of freedom and $\lambda_{i,j,m}^{(k)}$ is the non-centrality parameter, which depends on the channel impulse response at time index k and on $\mathsf{SNR}_{i,j}^{(k)}$. Let $F(e|\lambda_{i,j,m}^{(k)})$ and $f(e|\lambda_{i,j,m}^{(k)})$ denote the cumulative distribution function (CDF) and PDF of $\mathbf{b}_{i,j,m}^{(k)}$. The derivation of such probability functions and their parameters can be found in

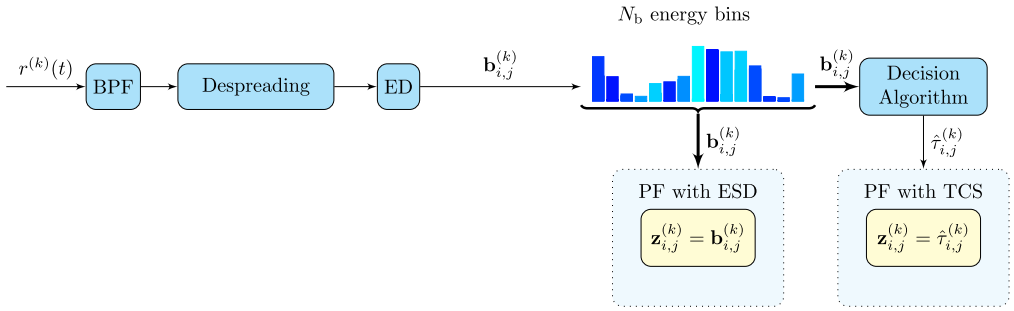

Fig. 4. Tag detection scheme with range-based least square, range-based BF, and energy profile-based BF.

[29], [38].

In the system under analysis, for the LS case we consider $\mathbf{z}_{l,i}^{(k)} = \widehat{\boldsymbol{\tau}}_{l,i}^{(k)}$ is the vector of round-trip times (RTTs). In particular, if the tag has been detected and identified by the reader, the TOA is estimated by a decision algorithm (e.g., by comparing the energy vector with a threshold) [26]. The algorithm for range-based LS is given in Alg. 1.

As for the BF, we consider two implementations depending on whether we use the raw energy samples $\mathbf{z}^{(k)} = \mathbf{b}^{(k)}$ or a TOA estimation taken from each energy vector $\mathbf{z}^{(k)} = \boldsymbol{\tau}^{(k)}$. The choice of $\mathbf{z}^{(k)}$ is driven by the knowledge of its probability distribution and the computational complexity, since it depends on the size of the dataset to be communicated in the network (e.g., in a centralized signal processing).

For range-based BF with $\mathbf{z}^{(k)} = \boldsymbol{\tau}^{(k)}$, the measurement model is given by

$$f(\widehat{\boldsymbol{\tau}}^{(k)}|\mathbf{x}^{(k)}) = \prod_{l\in\mathcal{R}}\prod_{i\in\mathcal{D}} \frac{1}{\sqrt{2\pi}\sigma_{\mathrm{p},k}} e^{-\frac{\left[\hat{\tau}_{l,i}^{(k)}\, c/2 - \|\mathbf{r}_l - \mathbf{x}_i^{(k)}\|\right]^2}{2\sigma_{\mathrm{p},k}^2}} \tag{30}$$

where $\mathbf{r}_l$ is the lth receiver position and $\mathcal{R}$ is the index set of receivers, $\sigma_{\mathrm{p},k}^2$ depends on the ranging techniques and the propagation conditions. The algorithm for range-based particle filter (PF) is given in Alg. 2.

For energy profile-based BF with $\mathbf{z}^{(k)} = \mathbf{b}^{(k)}$, the measurement model is given by

$$f(\mathbf{b}^{(k)}|\mathbf{x}^{(k)}) = \prod_{r\in\mathcal{R}}\prod_{m=1}^{N_\mathrm{bin}} f_{\mathbf{b}_{i,j,m}^{(k)}}\left(b_{i,j,m}^{(k)}\middle|\lambda_{i,j,m}^{(k)}\right) \tag{31}$$

where N_bin is the number of energy bins, $\sigma_{\mathrm{p},k}^2$ depends on the ranging techniques and the propagation conditions. Note that the dependence on $\mathbf{x}^{(k)}$ is hidden in $\lambda_{i,j,m}^{(k)}$, since this depends on $d_{i,j}^{(k)}$. The algorithm for energy profile-based PF is given in Alg. 3.

VI. Case Study

The validation of the proposed framework and signal processing techniques is made for a case study with an UWB RFID system working in an indoor scenario. To this aim, a measurement campaign has been carried out with one tag and one reader to collect a dataset of received signal samples. Based on such a dataset, the empirical measurement models have been extrapolated and used to simulate the OOA tracking of a stream of objects. We now present the experimental setup, the empirical measurement models, and the final results.

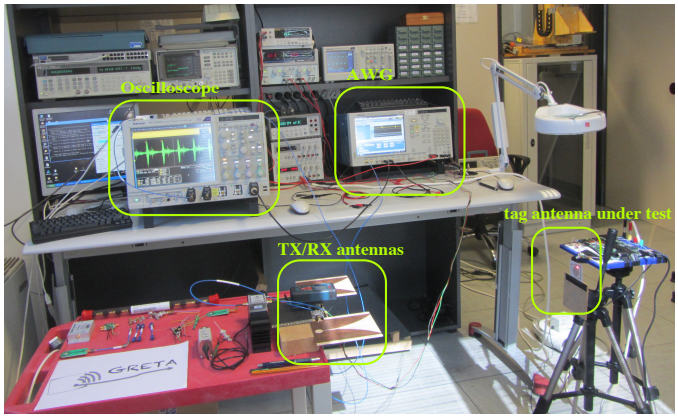

Fig. 5. Measurement setup.

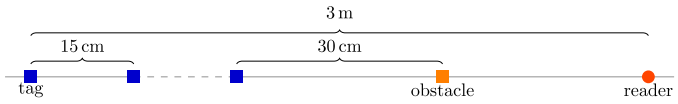

Fig. 6. Illustration of the system geometry used for collecting the measurements. The single tag has been deployed each time at a different position, from 0.6 m to 3 m distance from the reader with a step of 0.15 m. The measurements have been taken with and without an obstacle placed between the tag and the reader at a distance of 0.3 m from the tag.

TABLE II
Instrumentation used for measurements.

	Component	Producer	Model
Transmitter	AWG	Tektronix	AWG7122C
Receiver	Oscilloscope	Tektronix	DPO72304DX
Transmitter	Amplifier	Mini Circuits	ZVA-183X-S
Receiver	Amplifier (1)	Mini Circuits	ZVA-183X-S
Receiver	Amplifier (2)	Mini Circuits	ZVE-8G+
Receiver	Attenuator	Mini Circuits	RCDAT-6000-60
TX/RX	Antennas	Imego	Vivaldi 004
Tag	Switch	Hittite	104122-5
Tag	Control Logic	Microchip	PIC24FJ256DA210
Tag	Open load	Aeroflex	7006
Tag	Short load	Aeroflex	7008

A. Experimental Setup

The measurement setup is shown in Fig. 5. The probe transmitted signal is generated by an arbitrary waveform generator

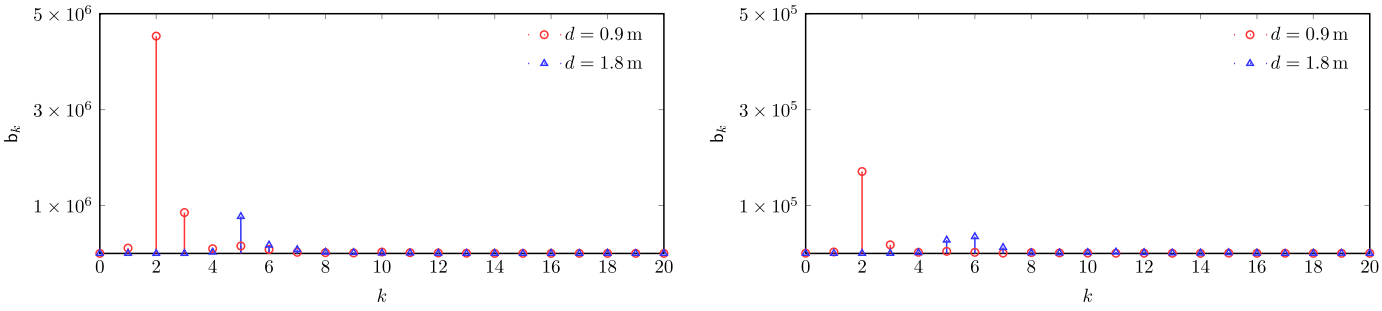

(a) line-of-sight (LOS) (b) NLOS

Fig. 7. Example of energy vectors obtained in LOS and NLOS conditions with $d = 90\,\mathrm{cm}$ (red) and $d = 180\,\mathrm{cm}$ (blue).

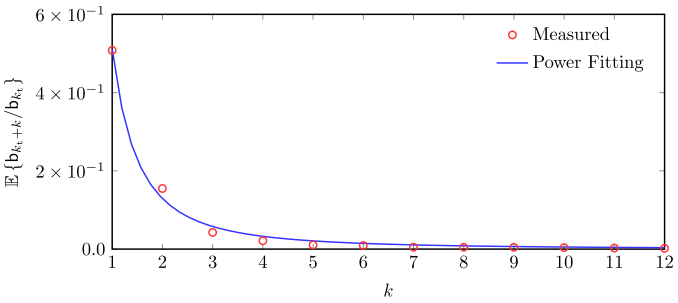

Fig. 8. Comparison of measurements and model for the average value of the normalized energy bin $\mathbf{b}_{k+k_\mathrm{t}}/\mathbf{b}_{k_\mathrm{t}}$ as a function of k. The power fitting model is $c_0(k-k_\mathrm{t})^{-\epsilon}$ with $c_0 = 0.51$ and $\epsilon = 1.98$.

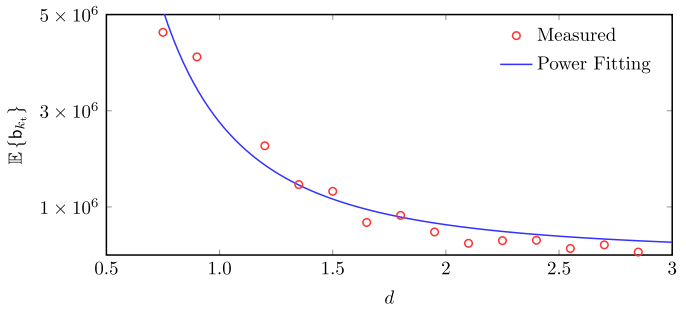

Fig. 9. Comparison of measurements and model for the average value of the energy bin $\mathbf{b}_{k_\mathrm{t}}$ as a function of the distance between tag and reader. The power fitting model is $e_0 d^{-\beta}$ with $e_0 = 2.76 \cdot 10^6$ and $\beta = 2.16$.

(AWG), amplified with a wideband amplifier and then fed to a wideband transmitting antenna. The radiated signal propagates in the environment and reaches the tag antenna under test. According to [41], it is necessary to implement a strategy to isolate the antenna mode component from the structural mode component and from the clutter at the receiver side. This is possible by changing the load connected to tag antenna according to the code $\{c_n\}$, which is accomplished by the connection of the tag antenna with a wideband switch, which is loaded with a short and an open circuit at its two ports.

The signal backscattered by the tag and by the surrounding environment is then collected by a receiving antenna, amplified, and then acquired by an oscilloscope. A programmable attenuator is inserted between the wideband amplifiers and the oscilloscope front-end in order to adapt the instrument dynamic to the amplitude of the incoming signal.

In the measurement setup (see Fig. 5) the receiving antenna and the transmitting antenna are close, forming a quasi-monostatic measurement configuration [24]. However, the presented measurement scheme can be applied to different transmitter/receiver antennas configurations, also separating them in space to test the backscattering characteristics of tags in bistatic configurations, which are very interesting for RFID applications [42]. Details on the instruments, antennas, amplifiers and tools adopted for the presented measurement setup are reported in Tab. II.

B. Empirical Measurement Models

We consider the PF algorithm for BF, which can outperform the extended Kalman filter (EKF) in non-Gaussian noisy observations [43], [44].[7] In particular, the position belief at time k is represented by a set of N_par random samples (particles) at $\{\mathbf{s}_s^{(k)}\}$, with $s = 1, 2, ..., N_\mathrm{par}$.

A dataset of measured energy bins has been collected for different values of $d_{i,j,m}^{(k)}$ between the tag and the reader as illustrated in Fig. 6. The same dataset has also been collected in NLOS conditions, by placing an obstacle between the tag and the reader.[8] The obstacle was at $0.3\,\mathrm{m}$ from the tag for each value of $d_{i,j,m}^{(k)}$ to simulate the presence of an object that precedes the one that is interrogated and moves with the same velocity vector. The UWB module emits pulses in the European lower band $[3.1, 4.8]\,\mathrm{GHz}$ with maximum power spectral density $-42\,\mathrm{dBm/MHz}$, in agreement with the IEEE 802.15.4 a standard [45].

Fig. 7(a) and 7(b) show examples of energy vector for $d_{i,j,m}^{(k)} = 0.9\,\mathrm{m}$ and $d_{i,j,m}^{(k)} = 1.80\,\mathrm{m}$ in LOS and NLOS conditions. It can be noticed the effect of distance and obstructed propagation in terms of energy loss.

From the collected dataset of measurements, an empirical model for the energy bins is extrapolated in the form of a power delay profile. To this aim, the bins are modeled as

$$\mathbf{b}_k = \begin{cases} n_\mathrm{n} & \text{for } 0 \le k < k_\mathrm{t} \\ e_0 d^{-\beta} + n_\mathrm{t} & \text{for } k = k_\mathrm{t} \\ e_0 d^{-\beta} c_0 (k-k_\mathrm{t})^{-\epsilon} + n_k & \text{for } k > k_\mathrm{t} \end{cases} \quad (32)$$

where $n_\mathrm{n} \sim \mathcal{N}(\mu_\mathrm{n}, \sigma_\mathrm{n}^2)$ is a Gaussian-distributed RV that depends only on noise; β is the path-loss exponent; $n_\mathrm{t} \sim$

[7] Note that, in general, the set of observations have a non-Gaussian distribution due to multipath and clutter residual.

[8] The obstacle was a box full of books.

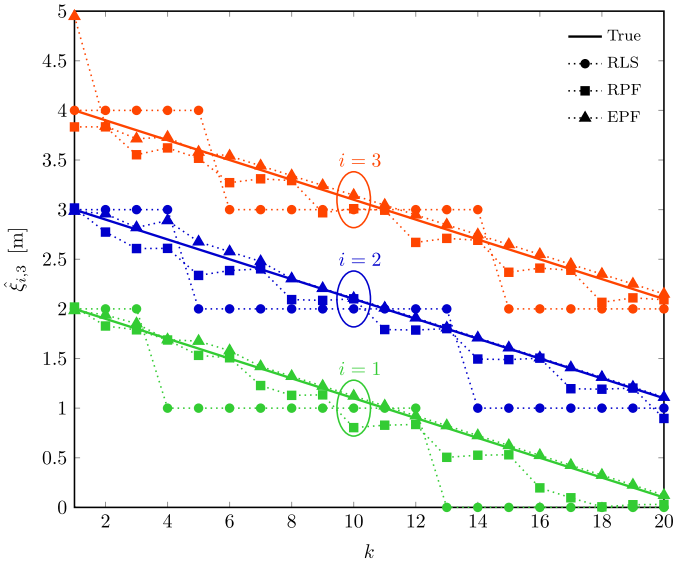

Fig. 10. The estimates $\hat{\xi}_{i,1}^{(k)}$ obtained with RLS, RPF, and EPF are compared with the true values $\xi_{i,1}^{(k)}$ (solid lines) for a stream of three objects and $N = 12$.

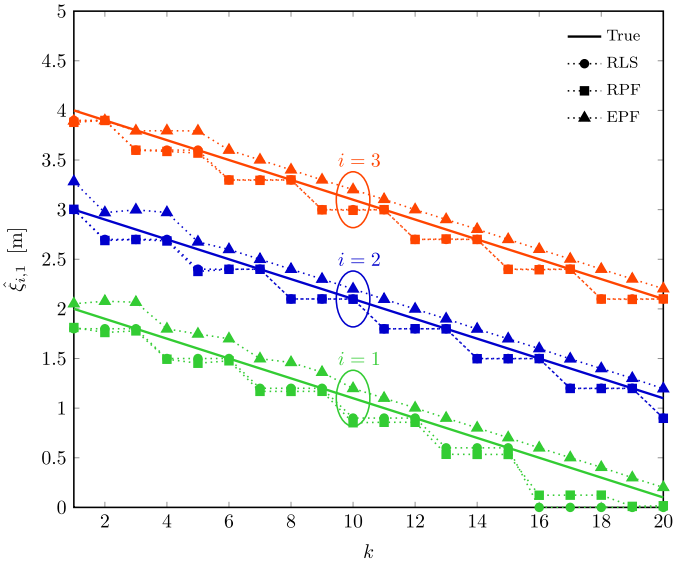

Fig. 11. The estimates $\hat{\xi}_{i,1}^{(k)}$ obtained with RLS, RPF, and EPF are compared with the true values $\xi_{i,1}^{(k)}$ (solid lines) for a stream of three objects and $N = 120$.

$\mathcal{N}(0, \sigma_{\mathrm{t}}^2)$ is a zero-mean Gaussian-distributed RV for the bin containing the first path; ϵ is the inter-bin decay constant; and $n_k \sim \mathcal{N}(0, \sigma_k^2)$ is a zero-mean Gaussian-distributed RV for the bin containing the undesired multipath.

The parameters $e_0, \beta, c_0, \epsilon, \mu_{\mathrm{n}}, \sigma_{\mathrm{n}}, \sigma_{\mathrm{t}}$, and σ_k have been extrapolated from the dataset of measured bins. Fig. 9 shows the curve fitting for the average value of the true bin of $\mathbf{b}_{k_{\mathrm{t}}}$ with the curve $e_0 d^{-\beta}$. Fig. 8 shows the curve fitting for the average value of $\mathbf{b}_k / \mathbf{b}_{k_{\mathrm{t}}}$ with the curve $c_0 (k - k_{\mathrm{t}})^{-\epsilon}$.

From the same dataset of energy samples, the relative TOA estimates $\hat{\boldsymbol{\tau}} = [\hat{\tau}_i]$ have been obtained through a threshold crossing search approach [29], [46], where the threshold is chosen with a constant false alarm rate (CFAR) method by setting the false-alarm probability to 10^{-2}. The empirical model has been assumed as Gaussian with mean and variance equal to the sample values. The empirical models for the energy samples and the TOA estimates will be used both for simulating an ordering problem with three objects and for determining the measurement models (30) and (31) for the BF. Therefore, the model for the energy bin is known.

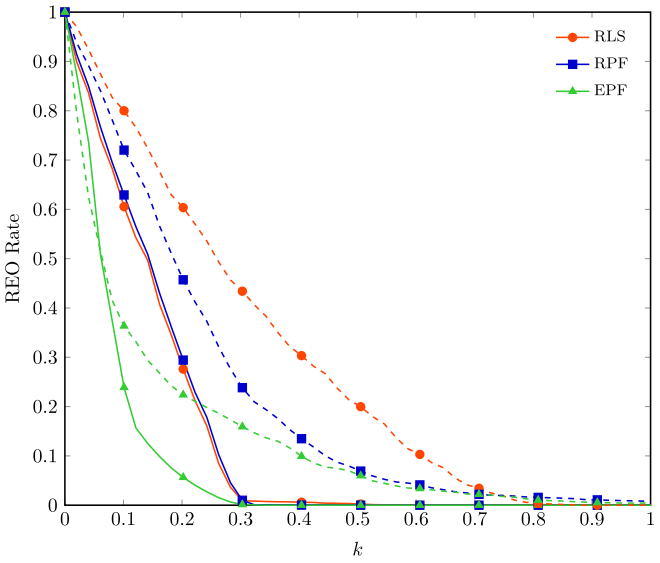

Fig. 12. Range error outage for $\xi_{i,1}^{(k)}$ obtained with the RLS, RPF, and EPF; the number of grid points and particles is $N = 12$ (dashed) and $N = 120$ (solid).

C. Results

Consider a stream of N_{o} objects equipped with a tag moving on a conveyor belt with $\dot{\mathbf{x}} = [v, 0, 0]$. The monitored area is a rectangular area of the conveyor of length $L = 5\,\mathrm{m}$ and width $W = 1\,\mathrm{m}$. A single reader is placed at the end of the area in position $\mathbf{r}$ and interrogates the three tags in order to estimate their order. In particular, we are interested in estimating the vector $\mathbf{o}$ by sorting the tag positions on the conveyor direction x. To this aim, we first estimate the vector of positions $\mathbf{x} = [\xi_1, \xi_2, \xi_3]$ with different algorithms: (1) the range-based least square (RLS); (2) the range-based particle filter (RPF); (3) the energy profile-based Particle filter (EPF). The algorithms are summarized in Alg. 1, Alg. 2, and Alg. 3, respectively. The LS algorithm is based on a fixed grid $\mathcal{G} \in \mathbb{R}^2$ composed of N_{g} points at position $\tilde{\mathbf{x}}_i$ with $i = 1, 2, \ldots, N_{\mathrm{g}}$ so that

$$\hat{\mathbf{x}}_{\mathrm{LS}} = \underset{[\tilde{\mathbf{x}}_1, \tilde{\mathbf{x}}_2, \ldots, \tilde{\mathbf{x}}_{N_{\mathrm{o}}}] \in \mathcal{G}^{N_{\mathrm{o}}}}{\operatorname{argmin}} \sum_{i=1}^{N_{\mathrm{o}}} (\hat{\tau}_i - \|\tilde{\mathbf{x}}_i - \mathbf{r}\|/c)^2 \,. \tag{33}$$

Therefore, $N = N_{\mathrm{par}} = N_{\mathrm{g}}$ is set for cases (2) and (3) to guarantee fair comparison. The energy-detector is set with $T_{\mathrm{dwell}} = 2\,\mathrm{ns}$; the corresponding spatial resolution is 30 cm (reader-tag-reader distance) in free space propagation.

Fig. 10 shows the estimated value for $\xi_{i,1}$ for case (1), (2), and (3) with $N = 12$. The LS algorithm shows the worst performance with the corresponding estimate $\xi_{i,1}$ presenting jumps due to the loose grid. On the other hand, the PF algorithm is not associated to a fixed grid thanks to the random

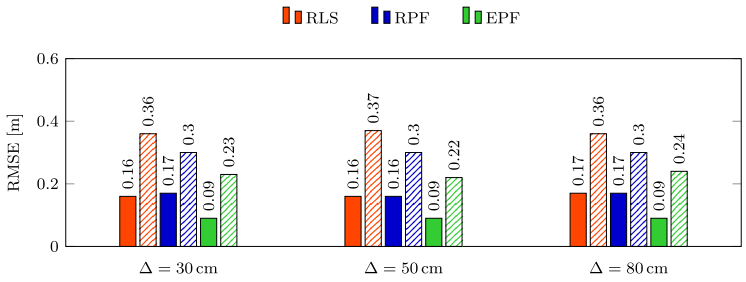

Fig. 13. Root mean squared error for $\hat{\xi}_{i,1}$ obtained by varying the distance between objects Δ and for $N = 12$ (dashed pattern) and $N = 120$ (solid pattern).

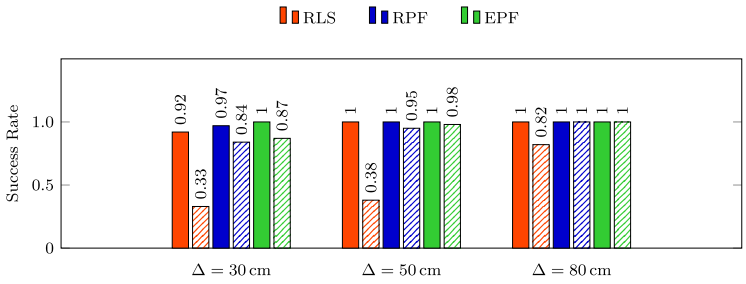

Fig. 14. Success rate obtained by varying the distance between objects Δ and for $N = 12$ (dashed pattern) and $N = 120$ (solid pattern).

resampling. Therefore, both the RPF and EPF outperform the RLS. However, the RPF strongly depends on the dwell time of the energy detector, which makes the TOA estimates belonging to a finite set of discrete values. Therefore, jumps are still present due to the time resolution of the TOA estimation. Finally, the EPF shows the best performance, also because it is not limited by any grid or resolution constraint in space or time. Fig. 11 shows the results under the same configuration as Fig. 10 for $N = 120$. In this case, the performance of the RLS algorithm is improved and is similar to that of the RPF. This results show that the prior knowledge of the mobility model allows the system to save resources in terms of computational complexity but most of all that the EPF case overcomes the resolution problems that arise in grid-based algorithms.

Fig. 12 shows the range error outage (REO) which is the probability for the range error of being above a certain value. The figure has been obtained with $N = 12$ and $N = 120$ and shows that the EPF outperforms the other algorithms for both the values of N. For example, for $N = 12$ the range error is above $0.20\,\mathrm{m}$ in the 32% of cases with EPF and in the 68% of cases for both RPF with the RLS. For $N = 120$ the range error is above $0.20\,\mathrm{m}$ in the 5% of cases with the EPF and in the 45% of cases for the RPF and 65% for the RLS.

Fig. 13 shows the RMSE for the estimation of $\xi_{i,1}$ for different values of Δ with $N = 12$ and $N = 120$. The EPF shows the minimum RMSE in all the configurations. The range-based RPF and RLS show similar values when $N = 120$, while the first outperforms the latter when $N = 12$. This is due to the fact that the LS accuracy is related to the grid of N equispaced points, while the range-based PF is related to the resolution of TOA estimation (i.e., the dwell time). Therefore, for $N = 12$ the resolution of the TOA estimation is finer than that of the least-square grid. For $N = 120$, the two resolutions are similar when mapped into the monitored area. This is also confirmed by Fig. 10 and Fig. 11.

Fig. 14 shows the relative success rate for the OOA tracking according to the definition of $P_{\mathrm{s}}(\mathbf{o})$ in (10). The success rate increases with Δ for all the three algorithms. In particular, all the object streams have been correctly sorted even with $\Delta = 0.3\,\mathrm{m}$ when the EPF is employed. Furthermore, the comparison with Fig. 13 for the RLS case with $N = 12$ shows that even if the RMSE is almost constant (about $0.36\,\mathrm{m}$) for all values of Δ, the success rate varies significantly from 0.33 to 0.82, showing that the success rate is more sensitive to variation of Δ with respect to the pure range error.

VII. Final Remark

A framework for design and analysis of RFID systems tracking the order-of-arrival (OOA) of objects is developed accounting for how network topology and wireless environment affects signals measurements and processing. A sorting decision problem is formulated and a tractable model for devising low-complexity method is derived. Based on a dataset of measurements collected through an experimental campaign with UWB-RFID, the performance of the proposed method is quantified and compared with that of other OOA tracking methods in an indoor environment. The proposed approach shows very good performance in terms of sorting success rate despite its low complexity. The outcomes of this work pave the way to a new OOA tracking methods for Industry 4.0.

Acknowledgment

References

[1] Z.-M. Liu and R. Hillegass, "A 3 patch near field antenna for conveyor bottom read in RFID sortation application," in *Proc. IEEE Antennas and Propag. Soc. Int. Symp.*, Albuquerque, NM, Jul. 2006, pp. 1043–1046.

[2] R. Siragusa, P. Lemaitre-Auger, A. Pouzin, and S. Tedjini, "RFID tags localization along an axis using a tunable near-field focused circular-phase array antenna," in *Proc. URSI General Assembly and Scientific Symp.*, Istanbul, Turkey, Aug. 2011, pp. 1–4.

[3] A. Buffi, P. Nepa, and F. Lombardini, "A phase-based technique for localization of UHF-RFID tags moving on a conveyor belt: Performance analysis and test-case measurements," *IEEE Sensors Journal*, vol. 15, no. 1, p. 387396, Jan. 2015.

[4] H. L. Van Trees, *Detection, Estimation, and Modulation Theory*, 1st ed. New York, NY 10158-0012: John Wiley & Sons, Inc., 1968.

[5] L. Shangguan, Z. Li, Z. Yang, M. Li, Y. Liu, and J. Han, "OTrack: Towards order tracking for tags in mobile RFID systems," *IEEE Trans. Parallel Distrib. Syst.*, vol. 25, no. 8, pp. 2114–2125, Aug 2014.

[6] Y. Choi, J. U. Won, and J. H. Park, "An experimental testbed for parcel handling with RFID technology," in *Int. Conf. on Adv. Commun. Techn.*, vol. 1, Feb 2006, pp. 320–326.

[7] D. Dardari, N. Decarli, A. Guerra, and F. Guidi, "The future of ultra-wideband localization in RFID," in *IEEE Int. Conf. on RFID*, Orlando, Florida, USA, May 2016, pp. 1–7.

[8] A. Costanzo, D. Masotti, T. Ussmueller, and R. Weigel, "Tag, you're it: Ranging and finding via RFID technology," *IEEE Microw. Mag.*, vol. 14, no. 5, pp. 36–46, Aug. 2013.

[9] P. Nepa, F. Lombardini, and A. Buffi, "Location and tracking of items moving on a conveyor belt and equipped with UHF-RFID tags," in *IEEE Antennas and Propag. Society Int. Symp. (APSURSI)*, Chicago, IL, Jul. 2012, pp. 1–2.

[10] P. Nikitin, R. Martinez, S. Ramamurthy, H. Leland, G. Spiess, and K. V. S. Rao, "Phase based spatial identification of UHF RFID tags," in *IEEE Int. Conf. on RFID*, Orlando, FL, Apr. 2010, pp. 102–109.

[11] B. R. Ray, M. U. Chowdhury, and J. H. Abawajy, "Secure object tracking protocol for the internet of things," *IEEE Internet of Things Journal*, vol. 3, no. 4, pp. 544–553, Aug. 2016.

[12] Y. Zhang, M. G. Amin, and S. Kaushik, "Localization and tracking of passive RFID tags based on direction estimation," *Hindawi Int. J. of Antennas and Propag.*, vol. 2007, pp. 1–9, 2007.

[13] M. Bolic, M. Rostamian, and P. M. Djurić, "Proximity detection with RFID: A step toward the Internet of Things," *IEEE Pervasive Comput.*, vol. 14, no. 2, pp. 70–76, Apr. 2015.

[14] L. Geng, M. Bugallo, A. Athalye, and P. Djurić, "Indoor tracking with RFID systems," *IEEE J. Sel. Topics Signal Process.*, vol. 8, no. 1, pp. 96–105, Feb. 2014.

[15] M. Z. Win and R. A. Scholtz, "Impulse radio: How it works," *IEEE Commun. Lett.*, vol. 2, no. 2, pp. 36–38, Feb. 1998.

[16] ——, "Ultra-wide bandwidth time-hopping spread-spectrum impulse radio for wireless multiple-access communications," *IEEE Trans. Commun.*, vol. 48, no. 4, pp. 679–691, Apr. 2000.

[17] Y. Shen and M. Z. Win, "Fundamental limits of wideband localization – Part I: A general framework," *IEEE Trans. Inf. Theory*, vol. 56, no. 10, pp. 4956–4980, Oct. 2010.

[18] S. Gezici, Z. Tian, G. B. Giannakis, H. Kobayashi, A. F. Molisch, H. V. Poor, and Z. Sahinoglu, "Localization via ultra-wideband radios: A look at positioning aspects for future sensor networks," *IEEE Signal Process. Mag.*, vol. 22, no. 4, pp. 70–84, Jul. 2005.

[19] A. Conti, M. Guerra, D. Dardari, N. Decarli, and M. Z. Win, "Network experimentation for cooperative localization," *IEEE J. Sel. Areas Commun.*, vol. 30, no. 2, pp. 467–475, Feb. 2012.

[20] A. Conti, D. Dardari, M. Guerra, L. Mucchi, and M. Z. Win, "Experimental characterization of diversity navigation," *IEEE Syst. J.*, vol. 8, no. 1, pp. 115–124, Mar. 2014.

[21] R. D'Errico, M. Bottazzi, F. Natali, E. Savioli, S. Bartoletti, A. Conti, D. Dardari, N. Decarli, F. Guidi, F. Dehmas, L. Ouvry, U. Alvarado, N. Hadaschik, C. Frankek, Z. Mhanna, M. Sacko, Y. Wei, and A. Sibille, "An UWB-UHF semi-passive RFID system for localization and tracking applications," in *IEEE Int. Conf. on RFID-Technology and Applications (RFID-TA)*, Nice, France, Nov. 2012, pp. 1–6.

[22] D. Dardari, R. D'Errico, C. Roblin, A. Sibille, and M. Z. Win, "Ultra-wide bandwidth RFID: The next generation?" *Proc. IEEE*, vol. 99, no. 7, pp. 1570–1582, Jul. 2010, special issue on *RFID - A Unique Radio Innovation for the 21st Century.*

[23] D. Arnitz, U. Muehlmann, and K. Witrisal, "UWB ranging in passive UHF RFID: Proof of concept," *IEEE Electronics Lett.*, vol. 46, no. 20, pp. 1401–1402, Oct. 2010.

[24] D. Dardari, F. Guidi, C. Roblin, and A. Sibille, "Ultra-wide bandwidth backscatter modulation: Processing schemes and performance," *EURASIP J. Wireless Commun. and Netw.*, pp. 1–15, Jul. 2011.

[25] S. Mazuelas, A. Conti, J. C. Allen, and M. Z. Win, "Soft range information for network localization," *IEEE Trans. Signal Process.*, vol. 66, no. 12, pp. 3155–3168, Jun. 2018.

[26] D. Dardari, A. Conti, U. J. Ferner, A. Giorgetti, and M. Z. Win, "Ranging with ultrawide bandwidth signals in multipath environments," *Proc. IEEE*, vol. 97, no. 2, pp. 404–426, Feb. 2009, special issue on *Ultra - Wide Bandwidth (UWB) Technology & Emerging Applications*.

[27] A. Rabbachin, I. Oppermann, and B. Denis, "ML time-of-arrival estimation based on low complexity UWB energy detection," in *Proc. IEEE Int. Conf. on Ultra-Wideband*, Waltham, MA, Sep. 2006, pp. 598–604.

[28] L. Stoica, A. Rabbachin, and I. Oppermann, "A low-complexity non-coherent IR-UWB transceiver architecture with TOA estimation," *IEEE Trans. Microw. Theory Tech.*, vol. 54, no. 4, pp. 1637–1646, Jun. 2006.

[29] S. Bartoletti, W. Dai, A. Conti, and M. Z. Win, "A mathematical model for wideband ranging," *IEEE J. Sel. Topics Signal Process.*, vol. 9, no. 2, pp. 216–228, Mar. 2015.

[30] S. Maranò, W. M. Gifford, H. Wymeersch, and M. Z. Win, "NLOS identification and mitigation for localization based on UWB experimental data," *IEEE J. Sel. Areas Commun.*, vol. 28, no. 7, pp. 1026–1035, Sep. 2010.

[31] A. Giorgetti and M. Chiani, "Time-of-arrival estimation based on information theoretic criteria," *IEEE Trans. Signal Process.*, vol. 61, no. 8, pp. 1869–1879, Apr. 2013.

[32] I. Guvenc, C. C. Chong, and F. Watanabe, "NLOS identification and mitigation for UWB localization systems," in *Proc. IEEE Wireless Commun. and Networking Conf.*, Hong Kong, Mar. 2007, pp. 3488–3492.

[33] S. Bartoletti, A. Giorgetti, M. Z. Win, and A. Conti, "Blind selection of representative observations for sensor radar networks," *IEEE Trans. Veh. Technol.*, vol. 64, no. 4, pp. 1388–1400, Apr. 2015.

[34] S. Bartoletti, A. Conti, and M. Z. Win, "Device-free counting via wideband signals," *IEEE J. Sel. Areas Commun.*, vol. 35, no. 5, pp. 1163–1174, May 2017.

[35] B. Denis and N. Daniele, "NLOS ranging error mitigation in a distributed positioning algorithm for indoor UWB ad-hoc networks," in *International Workshop on Wireless Ad-Hoc Networks*, Oulu, Finland, May/Jun. 2004, pp. 356–360.

[36] M. Z. Win, W. Dai, Y. Shen, G. Chrisikos, and H. V. Poor, "Network operation strategies for efficient localization and navigation," *Proc. IEEE*, vol. 106, no. 7, pp. 1224–1254, Jul. 2018, special issue on *Foundations and Trends in Localization Technologies*.

[37] M. Z. Win, Y. Shen, and W. Dai, "A theoretical foundation of network localization and navigation," *Proc. IEEE*, vol. 106, no. 7, pp. 1136–1165, Jul. 2018, special issue on *Foundations and Trends in Localization Technologies*.

[38] F. Guidi, N. Decarli, S. Bartoletti, A. Conti, and D. Dardari, "Detection of multiple tags based on impulsive backscattered signals," *IEEE Trans. Commun.*, vol. 62, no. 11, pp. 3918–3930, Nov. 2014.

[39] N. Decarli, F. Guidi, A. Conti, and D. Dardari, "Interference and clock drift effects in UWB RFID systems using backscatter modulation," in *Proc. IEEE Int. Conf. on Ultra-Wideband*, Syracuse, NY, Sep. 2012, pp. 1–5.

[40] F. Gustafsson and F. Gunnarsson, "Mobile positioning using wireless networks: possibilities and fundamental limitations based on available wireless network measurements," *IEEE Signal Process. Mag.*, vol. 22, no. 4, pp. 41–53, Jul. 2005.

[41] N. Decarli, A. Guerra, F. Guidi, M. Chiani, D. Dardari, A. Costanzo, M. Fantuzzi, D. Masotti, S. Bartoletti, J. S. Dehkordi, A. Conti, A. Romani, M. Tartagni, R. Alesii, P. D. Marco, F. Santucci, L. Roselli, M. Virili, P. Savazzi, , and M. Bozzi, "The GRETA architecture for energy efficient radio identification and localization," in *Proc. EURASIP Workshop on RFID Technology (EURFID)*, Oberaudorf, Germany, Oct. 2015, pp. 1–8.

[42] J. Kimionis, A. Bletsas, and J. N. Sahalos, "Increased range bistatic scatter radio," *IEEE Trans. Commun.*, vol. 62, no. 3, pp. 1091–1104, Mar. 2014.

[43] F. Gustafsson, F. Gunnarsson, N. Bergman, U. Forsell, J. Jansson, R. Karlsson, and P. J. Nordlund, "Particle filters for positioning, navigation and tracking," *IEEE Trans. Signal Process.*, vol. 50, no. 2, pp. 425–437, Feb. 2002.

[44] Y. Wang and P. M. Djurić, "Distributed Bayesian estimation of linear models with unknown observation covariances," *IEEE Transactions on Signal Processing*, vol. 64, no. 8, pp. 1962–1971, Apr. 2016.

[45] A. F. Molisch, D. Cassioli, C.-C. Chong, S. Emami, A. Fort, B. Kannan, J. Karedal, J. Kunisch, H. Schantz, K. Siwiak, and M. Z. Win, "A comprehensive standardized model for ultrawideband propagation channels," *IEEE Trans. Antennas Propag.*, vol. 54, no. 11, pp. 3151–3166, Nov. 2006, special issue on *Wireless Communications*.

[46] S. Bartoletti, A. Conti, W. Dai, and M. Z. Win, "Threshold profiling for wideband ranging," *IEEE Signal Process. Lett.*, vol. 25, no. 6, pp. 873–877, Jun. 2018.

Stefania Bartoletti (S'12–M'16) received the Laurea degree (*summa cum laude*) in electronics and telecommunications engineering and the Ph.D. degree in information engineering from the University of Ferrara, Italy, in 2011 and 2015, respectively.

Since June 2016, she is recipient of a Marie Skłodowska-Curie Global Fellowship within the H2020 European Framework for a research project with the Massachusetts Institute of Technology and the University of Ferrara. Her research interests include theory and experimentation of wireless networks for passive localization and physical behavior analysis. She is recipient of the 2016 Paul Baran Young Scholar Award of the Marconi Society.

Dr. Bartoletti served as a Chair of the TPC for the IEEE ICC Workshop on Advances in Network Localization and Navigation (ANLN) from 2017 to 2019, and as reviewer for numerous IEEE journals and international conferences.

Nicolò Decarli (S'10–M'14) received the Ph.D. degree in electronics, telecommunications, and information technologies from the University of Bologna, Italy, in 2013.

In 2012, he was a Visiting Student with the Wireless Communication and Network Sciences Laboratory, Massachusetts Institute of Technology, Cambridge, MA, USA. He is currently a Post-Doctoral Researcher with the Department of Electrical, Electronic, and Information Engineering, University of Bologna. His research interests include ultrawide bandwidth communications, radio localization, wireless sensor networks, and radio frequency identification.

Dr. Decarli serves as reviewer for numerous IEEE journals and conferences. In 2011 he served in the local organization committee of IEEE International Conference on Ultra Wideband (ICUWB). He was TPC co-chair of the 2018 IEEE ICC Workshop on Advances in Network Localization and Navigation (ANLN) and track-chair for 2018 IEEE International Symposium on Personal, Indoor and Mobile Radio Communications (PIMRC).

Davide Dardari (M'95–SM'07) is an Associate Professor at the University of Bologna, Italy. Since 2005, he has been a Research Affiliate at Massachusetts Institute of Technology, USA. His interests are on wireless communications, localization techniques and distributed signal processing. He published more than 200 technical papers and played several important roles in various National and European Projects. He received the IEEE Aerospace and Electronic Systems Societyś M. Barry Carlton Award (2011) and the IEEE Communications Society Fred W. Ellersick Prize (2012).

He is Senior Member of the IEEE where he was the Chair for the Radio Communications Committee of the IEEE Communication Society and Distinguished Lecturer (2018-2019). He was co-General Chair of the 2011 IEEE International Conference on Ultra-Wideband and co-organizer of the IEEE International Workshop on Advances in Network Localization and Navigation (ANLN) - ICC 2013-2016 editions. He was also TPC Chair of IEEE International Symposium on Personal, Indoor and Mobile Radio Communications (PIMRC 2018), TPC co-Chair of the Wireless Communications Symposium of the 2007/2017 IEEE International Conference on Communications, and TPC co-Chair of the 2006 IEEE International Conference on Ultra-Wideband. He served as an Editor for IEEE Transactions on Wireless Communications from 2006 to 2012 and as Guest Editor for several Journals.

Marco Chiani (M'94–SM'02–F'11) received the Dr. Ing. degree (summa cum laude) in electronic engineering and the Ph.D. degree in electronic and computer engineering from the University of Bologna, Italy, in 1989 and 1993, respectively. He is a Full Professor in Telecommunications at the University of Bologna. During summer 2001, he was a Visiting Scientist at AT&T Research Laboratories, Middletown, NJ. Since 2003 he has been a frequent visitor at the Massachusetts Institute of Technology (MIT), Cambridge, where he presently holds a Research Affiliate appointment.

His research interests are in the areas of communications theory, wireless systems, and statistical signal processing, including MIMO statistical analysis, codes on graphs, wireless multimedia, cognitive radio techniques, and ultra-wideband radios. In 2012 he has been appointed Distinguished Visiting Fellow of the Royal Academy of Engineering, UK. He is the past chair (2002–2004) of the Radio Communications Committee of the IEEE Communication Society and past Editor of Wireless Communication (2000–2007) for the journal IEEE TRANSACTIONS ON COMMUNICATIONS. He received the 2011 IEEE Communications Society Leonard G. Abraham Prize in the Field of Communications Systems, the 2012 IEEE Communications Society Fred W. Ellersick Prize, and the 2012 IEEE Communications Society Stephen O. Rice Prize in the Field of Communications Theory.

Andrea Conti (S'99–M'01–SM'11) received the Laurea (*summa cum laude*) in telecommunications engineering and the Ph.D. in electronic engineering and computer science from the University of Bologna, Italy, in 1997 and 2001, respectively.

He is an Associate Professor at the University of Ferrara, Italy. Prior to joining the University of Ferrara, he was with CNIT and with IEIIT-CNR. In Summer 2001, he was with the Wireless Systems Research Department at AT&T Research Laboratories. Since 2003, he has been a frequent visitor to the Wireless Information and Network Sciences Laboratory at the Massachusetts Institute of Technology, where he presently holds the Research Affiliate appointment. His research interests involve theory and experimentation of wireless systems and networks including network localization, distributed sensing, adaptive diversity communications, and network secrecy. He is recipient of the HTE Puskás Tivadar Medal and co-recipient of the IEEE Communications Society's Stephen O. Rice Prize in the field of Communications Theory and of the IEEE Communications Society's Fred W. Ellersick Prize.

Dr. Conti is an elected Fellow of the Institution of Engineering and Technology (IET). He has been the elected Chair of the IEEE Communications Society's Radio Communications Technical Committee. He is the Co-Founder and elected Secretary of the IEEE Quantum Communications & Information Technology Emerging Technical Subcommittee. He has served as an editor for the IEEE journals, as well as chaired international conferences. He has been selected as an IEEE Distinguished Lecturer.